Published in final edited form as:
J Phys Chem C Nanomater Interfaces. 2013 February 28; 117(8): 4268–4277. doi:10.1021/jp312031u.

Electrochemical Protease Biosensor Based on Enhanced AC Voltammetry Using Carbon Nanofiber Nanoelectrode Arrays

Luxi Z. Swisher[a], **Lateef U. Syed**[a], **Allan M. Prior**[a], **Foram R. Madiyar**[a], **Kyle R. Carlson**[a], **Thu A. Nguyen**[b], **Duy H. Hua**[a], and **Jun Li**[a,*]

[a]Department of Chemistry, Kansas State University, Manhattan, Kansas 66506, United States

[b]Department of Diagnostic Medicine/Pathobiology, College of Veterinary Medicine, Kansas State University, Manhattan, Kansas 66506, United States

Abstract

We report an electrochemical method for measuring the activity of proteases using nanoelectrode arrays (NEAs) fabricated with vertically aligned carbon nanofibers (VACNFs). The VACNFs of ~150 nm in diameter and 3 to 5 μm in length were grown on conductive substrates and encapsulated in SiO_2 matrix. After polishing and plasma etching, controlled VACNF tips are exposed to form an embedded VACNF NEA. Two types of tetrapeptides specific to cancer-mediated proteases legumain and cathepsin B are covalently attached to the exposed VACNF tip, with a ferrocene (Fc) moiety linked at the distal end. The redox signal of Fc can be measured with AC voltammetry (ACV) at ~1 kHz frequency on VACNF NEAs, showing distinct properties from macroscopic glassy carbon electrodes due to VACNF's unique interior structure. The enhanced ACV properties enable the kinetic measurements of proteolytic cleavage of the surface-attached tetrapeptides by proteases, further validated with a fluorescence assay. The data can be analyzed with a heterogeneous Michaelis-Menten model, giving "specificity constant" k_{cat}/K_m as (4.3 ± 0.8) × 10^4 $M^{-1}s^{-1}$ for cathepsin B and (1.13 ± 0.38) × 10^4 $M^{-1}s^{-1}$ for legumain. This method could be developed as portable multiplex electronic techniques for rapid cancer diagnosis and treatment monitoring.

Keywords

nanoelectrode array; legumain; cathepsin B; enzymatic kinetics; AC voltammetry

*Corresponding author: Telephone number: (785) 532-0955, Fax number: (785) 532-6666, junli@ksu.edu.

Author Contributions

The manuscript was written through contributions of all authors. All authors have given approval to the final version of the manuscript.

Supporting Information Available. FESEM image of VACNF NEA. Schemes for the syntheses of H_2N-$(CH_2)_4$CO-Ala-Ala-Asn-Leu-NHCH$_2$-Fc for legumain and H_2N-$(CH_2)_4$-CO-Leu-Arg-Phe-Gly-NH-CH_2-Fc for cathepsin B. The stability test of ACV of Fc-linked tetrapeptide attached on a macroscopic GCE. ACVs of cathepsin B tetrapeptide substrate H_2N-$(CH_2)_4$-CO-Ala-Ala-Asn-Leu-NH-CH_2-Fc immobilized on a macroscopic GCE and a VACNF NEA at different amplitudes of AC voltage. ACV peak current density $i_{p,acv}$ of cathepsin B tetrapeptide substrate H_2N-$(CH_2)_4$-CO-Leu-Arg-Phe-Gly-NH-CH_2-Fc immobilized on a VACNF NEA plotted against logarithm of the frequency and the amplitude of AC voltage. Negative control electrochemical experiments of cathepsin B study. Kinetic measurements and analyses of cathepsin B activity using the fluorescence assay. Negative control electrochemical experiments of legumain study. Kinetic measurements and analyses of legumain activity using the fluorescence assay. HPLC analyses of cathepsin B and legumain cleavage sites. Cyclic voltammetry of Fc-tetrapeptide functionalized on a GCE and a VACNF NEA. Specificity testing result of cathepsin B. This information is available free of charge via the Internet at http://pubs.acs.org.

Introduction

Proteases, the proteolytic processing proteins, are ubiquitous in living organisms and regulate a multitude of cellular processes including the cell cycle, hormone activation, apoptosis and angiogenesis.[1–3] The cysteine protease legumain, also known as asparaginyl endopeptidase (AEP), has a strict specificity for hydrolysis of asparaginyl bonds.[4] It is highly expressed in macrophages, on the cell surfaces and membranous vesicles in the metastatic and invasive solid tumors where it activates other proteases such as cathepsin B, H and L, that have both elastinolytic and collagenolytic activities.[5–7] In breast cancer, several recent studies have shown that absence of the cysteine protease inhibitor leads to increased growth and metastasis.[8] However, overexpression of those cysteine proteases was not found in the normal tissue. Thus, rapid detection of the presence and activity of cancer-mediated proteases (i.e. legumain and cathepsin B), should be developed for enhancement of treatment.[9]

Traditional methods for enzyme activity study include gel electrophoresis, high-performance liquid chromatography (HPLC), enzyme-linked immunosorbent assay (ELISA) and optical methods.[10–13] These methods require specific synthesis of peptides, fluorescent labels and sophisticated instrumentations, which are high-cost and time-consuming. Radioimmunoassay (RIA) had been widely used as an highly sensitive detection method but is diminished nowadays due to health safety and environment concerns.[14] Simple rapid electronic and/or electrochemical methods to detect enzyme activities are thus important in developing portable systems for point-of-care diagnosis and treatment monitoring of diseases such as cancers. Recently, electrochemical methods using cyclic voltammetric (CV) measurements of redox-labeled peptides attached on macroscopic gold electrodes have been demonstrated in detecting high-activity proteases such as trypsin, thrombin and plasmin.[15–16] Due to the localized sensing mechanism, an array of electrodes functionalized with different peptides could potentially detect multiple enzymes in a small sample volume. However, electrochemical detection of proteases that are more relevant to cancers, such as legumain and cathepsin B, has not been reported. These enzymes have much lower catalytic activity, making the measurement more difficult. Here we focus on a new electrochemical technique enabled by nanostructured electrodes that can successfully detect these enzymes.

It is well known that reducing the electrode size can dramatically enhance the detection sensitivity and temporal resolution of electrochemical measurements.[17–18] This trend extends from the scale of microns to nanometers. Well-separated nanoelectrode arrays (NEAs), either in regular pattern or in random distributions (also referred to as nanoelectrode ensembles (NEEs)), have attracted extensive interests for highly sensitive electroanalysis, measuring fast electrochemical kinetics, and biosensing.[19–21] Fabrication methods such as nanosphere lithography and E-beam lithography have been developed for the well-ordered NEAs.[22–23] Carbon based NEAs are particularly attractive for biosensors due to the wider applicable potential window and ease in biofunctionalization through robust covalent attachment. Development in this area, however, has been limited by the lack of readily available methods to fabricate reliable NEAs. Recent research in carbon nanotechnology has provided a method to fabricate well-controlled NEAs using vertically aligned carbon nanofibers (VACNFs) embedded in insulating materials.[24–26] Both precisely patterned and randomly distributed carbon nanofibers (CNFs) with the average diameter of 50–200 nm and uniform vertical alignment have been fabricated on 4″ Si wafers[27] and can be mass-produced into robust NEAs on individually addressed microelectrodes forming an “array-in-array” format. Various applications of VACNF NEAs with and without further encapsulation of insulating materials have been demonstrated for various biosensing or biomedical applications, including DNA hybridization analysis,[28] glucose detection,[25] electrochemical sensing of neurotransmitters,[29] neural electrical recording,[30] and gene

delivery.[31] Here we employ the embedded VACNF NEAs for enzymatic studies. The SiO_2 matrix was selectively etched by plasma etching to expose ~50–200 nm long CNF tips over the surface (as shown in Figure S1 in supporting Information). Specific peptide substrates were functionalized at the exposed CNF tips and subjected to proteolysis by proteases. The small radius of the CNF tips (~50–100 nm) protruding over the SiO_2 matrix makes it easier for enzymes to access to the peptides, avoiding the steric hindrance that is normally encountered on macroscopic surfaces.

Generally, CV measurements of bulk redox species using embedded VACNF NEAs show characteristic sigmoidal curves,[28,32] in which the tiny CNF tips carry much higher current densities than macro- or micro-electrodes. This feature indicates one of the predicted benefits of nanoelectrodes due to the nonlinear radial diffusion of redox species to the electrode surface.[33] The NEA also presents much smaller electrochemical cell time constant which allows the electrochemical measurement to be carried out at a much higher speed. These properties make NEAs attractive for rapid high-sensitivity biosensing applications.

Recently, we discovered that the electrochemical measurements on VACNF NEAs can be significantly improved by applying an alternating current (AC) voltage bias on the direct current (DC) ramps in the common CV measurement, i.e. by using AC voltammetry (ACV).[34] An anomalously high electron transfer rate was obtained with redox-active Fc molecules attached to the exposed CNF tips of the embedded NEAs.[34] This was attributed to the unique conically stacked graphitic structure of the CNFs, which opened a new capacitive pathway for AC current. As a result, ACV on VACNF NEAs can be carried out at much higher AC frequency (at kHz) than <100 Hz on macroscopic glassy carbon electrodes (GCEs). Since the magnitude of the signal in ACV, i.e. AC current amplitude, increases monotonically with the AC frequency at < 1 kHz, the detection sensitivity can be greatly enhanced using VACNF NEAs. The ACV is particularly advantageous over common CV for measuring small quantities of surface-attached redox molecules since the electrons can be shuffled back and forth for many times between the electrode and each adsorbed molecules. Here, we report the application of this property on detection of the enzymatic activities of legumain and cathepsin B by monitoring the kinetic decrease of the ACV signals of Fc attached to the CNF tip through a specific peptide linker during proteolysis. The data are well explained with the Michaelis-Menten heterogeneous enzymatic model.

Experimental Section

Apparatus and Reagents

The electrochemical measurements were conducted on a model 440A electrochemical analyzer (CH Instruments, Austin, TX). Fluorescence assay was performed on GloMax-Multi+ Microplate Multimode Reader (Promega Corporation, Madison, WI). A 96-well black polystyrene plate in the fluorescent measurement was from Whatman (Picataway, NJ). 3-Aminopropyl-triethoxysilane (APTES), 2-(2-methoxyethoxy)ethoxyacetic acid, 1-ethyl-3-(3-dimethylaminopropyl)carbodiimide hydrochloride (EDC), 1-hydroxy-2,5-dioxopyrrolidine-3-sulfonic acid sodium salt (sulfo-NHS), sodium hydroxides, and 6-amino-1-hexanol were purchased from Sigma-Aldrich (Saint Louis, MO). 2-(4-Morpholino)ethane sulfonic acid (MES) and dithiothreitol (DTT) were purchased from Thermo Fisher Scientific (Fair Lawn, NJ). Recombinant human legumain/asparaginyl endopeptidase (molecular weight of 49 kDa) and recombinant human cathepsin B (molecular weight of 29 kDa) were acquired from R&D Systems Inc. (Minneapolis, MN). Before use for enzymatic reactions, legumain was activated in an activation buffer, consisting of 50 mM CH_3COONa (pH 4.0, adjusted by adding acetic acid) and 100 mM NaCl. Cathepsin B was activated in an activation buffer of 5 mM DTT and 25 mM MES (pH 5.0). Substrates Z-Ala-Ala-Asn-AMC and Z-Leu-Arg-AMC for fluorescence assay

were obtained from Bachem (Torrance, CA). All aqueous solutions were prepared using 18.2 MP-cm resistivity deionized (DI) water from a bench-top water purifier (Barnstead EASYpure II RF/UV, Model D7035, Thermo Scientific, Asheville, NC).

Synthesis of Ferrocene-appended Tetrapeptides for Enzyme Cleavage

Ferrocene-appended tetrapeptide for legumain cleavage (i.e. H_2N-$(CH_2)_4$-CO-Ala-Ala-Asn-Leu-NH-CH_2-Fc) was synthesized following a sequence of reactions described in Figure S2. In brief, H-Leu-2-ClTrt-resin (Peptide International Inc., Louisville, KY) was converted to H-Ala-Ala-Asn-Leu-2-ClTrt-resin using a microwave peptide synthesizer (CEM Inc., Matthews, NC) by the sequence of reactions: (1) coupling with Fmoc-Asn-OH, *O*-(benzotriazol-1-yl)-*N,N,N′,N′*-tetramethyluronium hexafluorophosphate (HBTU), and diisopropylethylamine (DIEA) in DMF; (2) removal of the Fmoc protecting group with 20% piperidine in DMF; and (3) similarly, coupling with Fmoc-Ala-OH and removal of Fmoc twice using the same reagents as described above. H-Ala-Ala-Asn-Leu-2-ClTrt-resin was cleaved with trifluoroacetic acid (TFA), triisopropylsilane (TIPS), and water (95:2.5:2.5) to give H-Ala-Ala-Asn-Leu-OH, which upon protection of the amino function with di-*t*-butyl dicarbonate (Boc_2O) followed by the coupling with aminomethylferrocene[35] and 2-(7-aza-1*H*-benzotriazole-1-yl)-1,1,3,3-tetramethyluronium hexafluorophosphate (HATU) afforded Boc-Ala-Ala-Asn-Leu-$NHCH_2$Fc. Deprotection of the aforementioned tetrapeptide ferrocene with 10% TFA in dichloromethane at 25°C for 30 minutes, followed by condensation with *N*-Boc-5-aminovaleic acid and HATU in DMF, and removal of the Boc protecting group with 10% TFA in dichloromethane furnished H_2N-$(CH_2)_4$CO-Ala-Ala-Asn-Leu-$NHCH_2$-Fc. Ferrocene-labeled tetrapeptide substrate for cathepsin B cleavage (i.e. H_2N-$(CH_2)_4$-CO-Leu-Arg-Phe-Gly-NH-CH_2-Fc) was synthesized using a synthetic scheme similar to the aforementioned one and the details are described in Figure S3.

Fabrication of VACNF NEAs

The NEAs were fabricated by encapsulating VACNFs in SiO_2 matrix on a silicon chip using a similar method described in previous papers.[24,36] Briefly, VACNFs of an average length of ~5 μm were grown on ~100 nm Cr coated Si substrate using a DC-biased plasma enhanced chemical vapor deposition (PECVD) system (Aixtron, CA). A thin nickel film of ~22 nm was used as the catalyst to promote CNF growth. The electric field helped to align the CNF vertically on the substrate surface. Cross-sectional SEM images indicate that about 90% of the CNF have the length of 4 to 6 microns. The CNFs have the diameter distributed from ~100 to 200 nm and are well separated from each other, with an average distance of ~300 to 400 nm. Dielectric SiO_2 was deposited using chemical vapor deposition (CVD) from vapor-phase precursor tetraethylorthosilicate (TEOS) to fully encapsulate the bottom Cr metal contact layer and each individual CNFs. Mechanical polishing was applied using 0.3 μm alumina slurry to produce a flat surface. Reactive ion etching (RIE) with a mixture of CHF_3 and O_2 gases was then performed with NRE-3000 (Nano-Master Inc., Austin, TX) to selectively etch away desired amount of SiO_2. It can be controlled to expose 20% to 60% of the CNF tips based on the length variation. A typical VACNF NEA in this study consists of randomly distributed CNF tips with an average CNF diameter of ~100–200 nm and an average spacing over ~1 μm (corresponding to a density of ~$(1–10) \times 10^7$ CNFs-cm^{-2}). As shown in Figure S1, the length of exposed CNF tips was controlled at ~50–300 nm by varying the RIE time to selectively remove SiO_2.

Electrode Pre-conditioning

Before each use, VACNF NEAs were further polished with 0.05 μm γ-alumina slurry on napless polishing cloth (Buehler, Lake Bluff, IL) for 5–15 minutes, followed by rinsing with deionized water. The VACNF NEAs were then electrochemically activated by etching in 1.0

M NaOH solution using four cycles of CV in a potential range of −0.10 V to 1.20 V (vs. Ag/AgCl (3 M KCl)) at a scan rate of 50 $mV \cdot s^{-1}$.

Passivation of the SiO_2 Surface of the VACNF NEA Chip

To reduce nonspecific adsorption, the SiO_2 surface of the VACNF NEAs was first passivated with protective moieties containing ethylene glycol. The chip was immersed in an 8 g L^{-1} solution of APTES in ethanol for 20 minutes to produce a primary amine derivatized surface. The chip was treated with 50 μL solution of 0.1 mM of 2-(2-methoxyethoxy)ethoxyacetic acid, 100 g L^{-1} of EDC and 50 g L^{-1} of sulfo-NHS, and incubated at room temperature for 2 hours in an enclosed chamber (Arrayit, CA). The carboxylic acid group of 2-(2-methoxyethoxy)ethoxyacetic acid formed an amide bond with the amino function on the chip surface, leaving ethylene glycol moiety covering the surface. The molecules attached to the CNF tips were then removed by electrochemical etching at 1.2 V (vs. Ag/AgCl (3 M KCl)) for 20 seconds in 1.0 M NaOH solution. This process regenerated clean CNF tips which contain abundant carboxylic acid functional groups.

Functionalization of the VACNF NEA Chip

The tetrapeptide H_2N-$(CH_2)_4$-CO-Ala-Ala-Asn-Leu-$NHCH_2$-Fc for legumain study or H_2N-$(CH_2)_4$-CO-Leu-Arg-Phe-Gly-NH-CH_2-Fc for cathepsin B study was covalently linked to the VACNF NEA by forming amide bond facilitated by EDC and sulfo-NHS. Typically, a solution of 10 μL of 10 mM tetrapeptide mixed with 90 μL of 10 g L^{-1} EDC and sulfo-NHS was applied onto the electrochemically activated VACNF NEA chip and incubated in the enclosed Arrayit chamber at room temperature for 2 hours. Control experiments and HPLC-MS characterization (see Supporting Information) confirmed that only the end $–NH_2$ group of the tetrapeptide formed amide bond with the carboxylic acid group on the VACNF NEA. The $–NH_2$ and NH functions in asparagine and arginine moieties in the peptide do not react with the carboxylic acid group under the reaction conditions. In order to stabilize the electronic signal, the CNF electrode surface was further dipped into a solution of 5 mL of 1 mM 6-amino-1-hexanol containing 5 g L^{-1} EDC and 2 g L^{-1} sulfo-NHS so that the unreacted –COOH sites were linked with 6-aminohexanol.

Electrochemical Measurements

The electrochemical measurements were performed in a TEFLON cell with a total volume of 250 μL. The cell was sealed against a VACNF NEA chip with a 3-mm i.d. O-ring in a three-electrode configuration with the VACNF NEA as the working electrode, an Ag/AgCl (3M KCl) reference electrode and a coiled Pt wire as the counter electrode. The electrolyte solutions were consisted of 50 mM MES (pH = 5.0) and 250 mM NaCl for legumain experiment and 25 mM MES (pH = 5.0) for cathepsin B experiment. The average AC current was measured by applying an AC voltage bias on the DC staircase waveform with the potential sweeping from −0.05 to +0.65 V for legumain experiment and −0.1 V to +0.75 V for cathepsin B experiment, both at 10 $mV \cdot s^{-1}$ scan rate. The parameters including AC voltage amplitude and frequency were varied in specific experiments and specified as the results are presented in later sections.

Validation of the Enzyme Activities with Other Biochemical Methods

The activities of the enzymes vary significantly from batch to batch and are very sensitive to the environment and storage conditions. To reduce the errors, all enzymes were first validated with an established fluorescence-based biochemical method before each electrochemical experiment. The legumain activity was measured with a kinetic fluorescence assay using a commercial substrate Z-Ala-Ala-Asn-AMC which gave strong fluorescence after cleavage at the site between asparagine and AMC dye. The substrate Z-

Leu-Arg-AMC was used in the fluorescence assay for cathepsin B activity measurement. The cleavage at the site between arginine and AMC dye released the AMC from quenching by the carbonyl group and showed increased fluorescence intensity.

Results and Discussion

The Design and Electrochemical Characterization of VACNF NEAs for Protease Detection

Scheme 1 shows the structure of an embedded VACNF NEA covalently attached with Fc-linked peptides at the exposed CNF tips. The Fc moiety at the distal end provides a reliable redox signal at ~0.25 V vs. Ag/AgCl (3M KCl) in ACV measurements. Upon supplied with the specific protease, the peptide is expected to be cleaved at the particular site. As a result, the Fc moiety is released from the electrode surface into the bulk solution, causing the redox signal to decrease. The kinetic of the enzymatic reaction at the electrode surface will be monitored by continuously repeated ACV measurements. The advantage of this method is that the appended Fc moiety provides a characteristic faradaic signal which can be easily separated from the unstable nonfaradaic background and other interfering redox signals. The key for this method is that the Fc signal needs to be relatively large and stable over the period of the kinetic measurements (up to ~1 hour) and the ACV measurement at each point is fast enough to provide ~1 minute (or less) of temporal resolution. This may become challenging for enzymes requiring long peptide substrate sequences for specific recognition. The Fc signal involves electron transfer between Fc molecule and the electrode surface, which is highly sensitive to the Fc-surface distance and the molecular packing of the peptides on the electrode surface. Thus the electrochemical properties of Fc-linked peptide attached on VACNF NEAs need to be carefully characterized.

Figure 1 shows the comparison of ACVs of a macro-GCE and a VACNF NEA, both functionalized with the tetrapeptide H_2N-$(CH_2)_4$-CO-Ala-Ala-Asn-Leu-$NHCH_2$-Fc to be used for legumain study. A peak current was observed at ~0.2 V vs. Ag/AgCl (3M KCl) for both electrodes. The amplitude of the peak current density (i_p) in the ACVs with macro-GCE increased from ~1.0×10^{-7} A•mm^{-2} at 10 Hz to ~2.0×10^{-7} A•mm^{-2} at 40 Hz, but then dropped to zero at 1500 Hz. At the meantime, the background signal steadily increased from ~4.7×10^{-7}, to 1.8×10^{-6} and 2.8×10^{-6} A•mm^{-2}, respectively. In contrast, although the i_p of ACV with VACNF NEAs was not measurable at 10 Hz and 40 Hz, it rose clearly above the background at 1500 Hz, giving ~2.0×10^{-8} A•mm^{-2}. Obviously, VACNF NEAs allowed the Fc signal to be detected at much higher frequency. It is noteworthy that the current density in Figure 1 was calculated with the geometric electrode surface area. As shown in Figure S1, the actual exposed CNF surface area in the VACNF NEA is more than ~100 times less than the geometric surface area. Hence the real current density at the CNF tip is at least 10 times higher than that at the GCE. Generally, the electrochemical signal is very sensitive to Fc-surface distance since the electron transfer rate decays exponentially versus the Fc-surface distance. Hence electrochemical sensors based on redox reactions normally use linker molecules less than 2 nm in length. Here, the electron transfer on both GCEs and VACNF NEAs was not significantly affected by the tetrapeptide and the linker (with a fully extended length of ~2.5 nm). Experiments with an even longer octapeptide (to be published) did not show notable difference in Fc signal, suggesting that the molecule might be folded back to the CNF surface.

ACV uses a sinusoidal AC voltage superimposed on a DC potential ramp for voltammetric measurements. It has advantages over commonly used DC-based CV, particularly for biosensors, due to the ability to amplify the electrochemical signal of small quantity of redox tags by shuffling the electron between the redox tag and the electrode many times. In general, the signal increases with AC frequency at low frequencies but is saturated and then decreases at higher frequencies. In our previous study using VACNF NEAs, the optimum

frequency for Fc through a short NH_2CH_2- linker was found to be 40 times higher than that on the macro-GCE.[34] Figure 2 illustrates the similar phenomena with Fc attached to the electrode surface through the tetrapeptide and a longer linker group versus the AC frequency. Clearly, the optimum frequency which gave the maximum i_p was 40 Hz for the GCE, but 1750 Hz for the VACNF NEA. Despite that both frequency values are about half of those with short NH_2CH_2-linker, the drastic difference between VACNF NEA and macro-GCE remained the same, i.e. the optimum frequency on the VACNF NEA was ~40 times of that on the GCE. The higher applicable AC frequency at VACNF NEA afforded a larger ACV signal (i.e. i_p) and faster ACV measurements. Each ACV measurement in Figure 1 can be done in ~60–70 s. As a result, the kinetics of enzymatic cleavage can be monitored with continuously repeated ACV measurements at a temporal resolution of ~1 minute.

The AC peak current density $i_{p,acv}$ can be extracted by subtracting the background (as a simple sloped straight line). These values are plot in Figure 2a versus the AC frequency. Clearly, the AC peak current density of the GCE shows a sharp peak with the maximum at 40 Hz and a full width at half maximum (FWHM) of ~140 Hz. The current value approximately increases linearly with the AC frequency but drops rapidly as the AC frequency exceeds 40 Hz. In contrast, the maximum AC peak current density was observed at 1750 Hz on the VACNF NEA and the FWHM asymmetrically spread over 5000 Hz, indicating a large range of frequency that can be used. The current density increases about linearly with the frequency up to ~1000 Hz. When the peak current density is plot versus the logarithm of the AC frequency as shown in Figure 2b, the curves obtained with the GCE and the VACNF NEA show similar shape but with shifted peak frequency. It needs to be noted that the ACV measurements are not stable with the GCE. The peak shape changed significantly in about 10 minutes as shown in Figure S4, which limits the use of GCEs for the measurement of enzymatic kinetics. In contrast, the peak shape of the ACV curve of VACNF NEAs is much more stable.

The peak current in ACVs also depended on the amplitude of the applied AC voltage. Figure 3 shows that there is a small difference between the GCE and the VACNF NEA. The peak current density ($i_{p,acv}$) reached to the highest value of ~1.5×10^{-6} A•mm^{-2} at the amplitude of 0.35 V for GCE while the peak current density kept increasing at the amplitude up to 0.50 V for VACNF NEA. However, for the VACNF NEA at amplitude larger than 0.15 V, the value of the peak current density deviated from the linear relationship and the raw ACV peak became broad and unstable (Figure S5). For this reason, we choose amplitude at 0.15 V as the optimum working amplitude in all the following ACV measurements for legumain activity study. For cathepsin B study, the tetrapeptide H_2N-$(CH_2)_4$-CO-Leu-Arg-Phe-Gly-NH-CH_2-Fc was immobilized on the VACNF NEA, giving very similar ACV properties with slightly different optimum AC frequency (800 Hz) and amplitude (0.15 V), respectively (see Figure S6). These optimum parameters were used in the following kinetic study on cathepsin B activities.

Figure 4a shows the change of peak current ($i_{p,acv}$) over time during continuously repeated ACV measurements with Fc-linked tetrapeptide (H_2N-$(CH_2)_4$-CO-Leu-Arg-Phe-Gly-NH-CH_2-Fc) immobilized on a VACNF NEA. The initial signal was quite stable, with only slow drifting. At ~20 minute, a solution of 25 μL of 9.8 ng•μL^{-1} (338 nM) cathepsin B in the activation buffer was added into the electrochemical cell, giving a final enzyme concentration of 30.7 nM. Due to the disturbance to in electrolyte, the ACV peak current jumped up and then followed by an exponential decay. Figure 4b shows the ACV curve measured at 20 minute, immediately after the cathepsin B solution was added. A clear peak at around 0.25 V confirms the immobilization of Fc-linked tetrapeptide on the electrode surface. Figure 4c further illustrates the representative background-subtracted ACV curves

corresponding to 0, 5, 10, 20 and 55 minutes, respectively, after adding the cathepsin B solution. The peak current clearly decreased over time and the peak position slowly shifted from 0.27 V to 0.18 V. Two control experiments (Figure S7) were carried out and confirmed that the exponential decay in $i_{p,acv}$ was truly attributed to the kinetics of enzymatic cleavage of the peptide. First, 25 μL of blank activation buffer, i.e. 5 mM DTT and 25 mM MES (pH 5.0), was added into the electrochemical cell prefilled with 250 μL of electrolyte (25 mM MES (pH 5.0)). The disturbance to the ACV signal was negligible in this process. Second, a solution of 25 μL of activation buffer containing deactivated cathepsin B (which was confirmed with the fluorescence assay) was added into the electrochemical cell in the similar way as in the first case. Neither case showed the characteristic exponential decay observed when the activated enzyme was introduced. It is clear that the exponential decay was due to enzymatic cleavage to the tetrapeptide substrate by cathepsin B.

The observed proteolysis kinetics may be explained with a modified Michaelis-Menten model for heterogeneous enzymatic reactions:[37]

$$E+S_s \underset{k_{-1}}{\overset{k_1}{\longleftrightarrow}} \mathrm{ES}_s \xrightarrow{k_{cat}} E+P_s+P, \quad (1)$$

where E, S_s, ES_s, P_s and P represent the enzyme, the surface-bound peptide substrate, the enzyme-substrate complex on the electrode surface, the surface-attached product, and the product released to solution, respectively. The reaction rate can be defined as

$$\upsilon=-\frac{d\Gamma_{Ss}}{dt}=\frac{d\Gamma_{Ps}}{dt}=\frac{k_{cat}[E_0]\times\Gamma_{Ss}}{K_m+[E_0]}, \quad (2)$$

where k_{cat} is the dissociation rate constant, $K_m = (k_{cat}+k_{-1})/k_1$ is the Michaelis-Menten constant, and Γ_{Ss} and Γ_{Ps} represent the surface densities of original and reacted peptide substrates, respectively. At low enzyme concentrations with $[E_0] \ll K_m$, an approximate relationship can be obtained as

$$\upsilon=-\frac{d\Gamma_{Ss}}{dt}=\frac{d\Gamma_{Ps}}{dt}=\frac{k_{cat}}{K_m}[E_0]\times\Gamma_{Ss}. \quad (3)$$

The reaction rate υ (or $-d\Gamma_{Ss}/dt$) is a time-dependent quantity proportional to the change in electrochemical signals (dS/dt), where S is the kinetic electrochemical signal corresponding to the peak current i_p in ACV measurements. As a result the slope of (dS/dt) versus the time-dependent Γ_{Ss} will be equal to (k_{cat}/K_m)[E_0], namely

$$-\frac{d\Gamma_{Ss}/dt}{\Gamma_{Ss}}=-\frac{dS/dt}{S}=\frac{k_{cat}}{K_m}[E_0]. \quad (4)$$

Thus, by rearranging the kinetic electrochemical data, we can derive the value of "specificity constant" k_{cat}/K_m which is commonly used to represent the catalytic efficiency of enzymes.

To further analyze the kinetic enzymatic process, the peak current in ACV was converted into the quantity of surface adsorbed Fc (i.e. Γ_{surf}) based on[38]

$$i_{p,acv}=\left(\frac{2}{\pi}\right)\left(\frac{F^2}{4RT}\right)\Gamma_{surf}(2\pi f)V_0, \quad (5)$$

where the AC frequency f was 800 Hz and the amplitude of the AC voltage V_0 was 150 mV. Although the Γ_{surf} value derived with Equation 5 is known to be smaller than that obtained with other methods, particularly at high frequencies, the linear relationship between $i_{p,acv}$ and Γ_{surf} remains true. The deviation of the proportional coefficient from the true value is cancelled in later steps and does not affect the final results. As shown in Figure 5a, the kinetic data can be fitted with an exponential decay superimposed on a linear curve corresponding to the slow baseline drift. The fitting equation is

$$\Gamma_{surf}=1.55\times10^{-15}\times e^{\left(-\frac{t}{683.6}\right)}-2.19\times10^{-19}t+1.38\times10^{-15}. \quad (6)$$

From equation 6, the reaction rate v_i at different Γ_{surf} can be calculated. The results were presented in Figure 5b, which appeared to be a linear curve in the high Γ_{surf} region. This linear curve is fitted by equation

$$v_i=1.15\times10^{-3}\Gamma_{surf}-1.20\times10^{-18}. \quad (7)$$

As mentioned earlier, both v_i and Γ_{surf} are proportional to $i_{p,acv}$. The slope of v_i versus Γ_{surf}, however, is independent of the exact proportional coefficient since it presented in both v_i and Γ_{surf} and is thus cancelled. Therefore, we can derive the exact slope without being affected by the ACV experimental conditions. Equation 7 gives a slope of 1.15×10^{-3} s^{-1}, which equals to $(k_{cat}/K_m)[E_0]$ as described in Equation 3. With $[E_0]$ = 30.7 nM, the value of the "specificity constant" k_{cat}/K_m can be calculated as 3.8×10^4 $M^{-1}s^{-1}$. This value is close to the value of 2.3×10^4 $M^{-1}s^{-1}$ derived from the comprehensive analysis with the fluorescence assay in a series of peptide substrate concentrations (Figures S8 and S9). It is also within the range reported in literature which varies from ~2×10^3 $M^{-1}s^{-1}$ to ~7×10^6 $M^{-1}s^{-1}$.[37, 39–40]

Figure 6 shows the ACV measurements with H_2N-$(CH_2)_4$-CO-Ala-Ala-Asn-Leu-NH-CH_2-Fc immobilized on a VACNF NEA. Comparing to cathepsin B, the change of peak current corresponding to the cleavage by legumain was smaller, likely due to the difference in the enzyme activity. None of the two control experiments in Figure S10 by adding the blank activation buffer and the buffer containing deactivated legumain (confirmed with fluorescence assay), respectively, showed the characteristic exponential decay in $i_{p,acv}$. The former caused negligible disturbance to the electrochemical signal. The latter caused the $i_{p,acv}$ to slowly rise by ~5% after 5 minutes and then became stabilized, which might be attributed to the disturbance to the tetrapeptide conformation on the electrode surface.

The data in Figure 6b can be fitted with the following equation:

$$\Gamma_{surf}=3.23\times10^{-16}\times e^{\left(-\frac{t}{1101}\right)}-4.36\times10^{-20}t+3.75\times10^{-15} \quad (8)$$

where the time constant is 1101 s (~18 min.), indicating that the reaction is quite slow. It normally took ~1 hour to complete the kinetic measurement. This was found to be limited by the low enzymatic activity of legumain. However, it was still possible to extract the faradaic signal of Fc from the varying background with the ACV measurements. Figure 6c gives a linear curve fitted by equation $v_i=6.30\times10^{-4}\Gamma_{surf}-2.30\times10^{-18}$ with the slope of 6.30×10^{-4} s^{-1} at $[E_0]$ = 80.1 nM. From this analysis, the value of the k_{cat}/K_m can be

calculated as $7.9 \times 10^3\ M^{-1}s^{-1}$. This value is higher than the value of $4.3 \times 10^3\ M^{-1}s^{-1}$ derived from the comprehensive analysis using the fluorescence assay (Figures S11 and S12) and the specifications provided by the vendor (R&D Systems).

The kinetic measurements with ACV for both cathepsin B and legumain were repeated at least three times under similar conditions as those in Figure 4 and Figure 6. The results were consistent and reproducible. More comprehensive measurements at varied enzyme concentrations and peptide lengths will be reported in future studies. Table 1 summarizes the statistical values of the specificity constant k_{cat}/K_m derived from both electrochemical method using ACVs on VACNF NEAs in comparison with the fluorescence assay based on a series of substrate concentrations in solution, for both legumain and cathepsin B. Interestingly, the electrochemical method gave higher k_{cat}/K_m values for both of legumain and cathepsin B than the fluorescence assay. In contrast, other studies using macroscopic electrodes found that the electrochemically measured k_{cat}/K_m was normally lower than solution based assays, primarily due to the steric effects which lower the access of enzyme to the peptides attached to the flat surface.[15–16] The results confirmed that the small radius in VACNF NEAs helped to eliminate the steric hindrance. The peptide substrates for the fluorescence assay consisted of only 3 and 2 amino acids, respectively, which were also expected to have lower binding affinity than the tetrapeptides used for our electrochemical measurements.

The values of the specificity constant k_{cat}/K_m for cathepsin B by both electrochemical and fluorescence assays are about 5 times of that of legumain. For ACV measurements, this helps to reduce the time constant for the exponential decay and makes the experiment easier and more reliable. As a result, lower enzyme concentration can be measured. From these results, it can be concluded that the ACV would work even better for measuring proteases with the k_{cat}/K_m values higher than $\sim 4 \times 10^4\ M^{-1}s^{-1}$. But even proteases with relatively low specificity constant (such as legumain and cathepsin B) can still be reliably measured. Even though the required enzyme concentration was ~5 to 10 times higher than that by the fluorescence assay, the electrochemical method has a potential advantage that simultaneous detection of multiple proteases in a small volume is possible, attributed to its localized sensing mechanism using surface-attached peptides. Further investigation is in progress to assess the cross-reactions between different enzyme-substrate pairs.

The vendor suggests that legumain cleaves peptide bonds with asparagine (Asn) at the P1 position while it has been reported that cathepsin B cleaves peptide or AMC bonds with arginine (Arg) at P1 site.[41] To confirm the cleavage site, we have incubated each tetrapeptide with legumain and cathepsin B and measured the products with HPLC. As shown in Figure S13 and Figure S14, the HPLC graphs of the cleaved products were directly compared with those of the pure tetrapeptides and synthesized fragments (mono amino acid or dipeptide). The cleaved products were further validated with mass spectrometry. These experiments clearly demonstrated the cleavage site as listed in Table 1. Interestingly, even after incubating for 2 hours, the cleaved tetrapepetide concentration was only ~1/5 of the total concentration for legumain and ~3/4 for cathepsin B. The fluorescence assay reported earlier is sensitive to the absolute amount of cleaved products while the electrochemical assay is sensitive to the percentage of the cleavage to the surface-attached peptide. The large amount of starting peptides used in the fluorescence assay partially contributed to its capability to measure lower enzyme concentrations. The electrochemical method, however, has advantage for miniaturization and multiplexing which may be critical for rapidly screening multiple proteases in disease diagnosis. It is noteworthy that the k_{cat}/K_m values of legumain and cathepsin B are relatively low, but they have high biological significance respect to cancer diagnosis and treatment. The speed and required enzyme concentration in the electrochemical measurements can be significantly improved when this technique is used

to detect other proteases with higher k_{cat}/K_m values, such as trypsin at $(1.44 \pm 0.1) \times 10^6$ $M^{-1}s^{-1}$,[15] α-thrombin at $(1.0 \pm 0.2) \times 10^6$ $M^{-1}s^{-1}$,[15] and plasmin at 6.7×10^5 $M^{-1}s^{-1}$.[16]

In previous electrochemical detection of proteases including trypsin,[15] a-thrombin,[15] and plasmin,[16] normal CV measurements on gold electrodes were used. This method was found not applicable on carbon electrode. As shown in Figure S15, the Fc redox waves of the labeled tetrapeptide can be observed on the GCE, but the baseline currents were quite high, making it difficult to reliably extract redox signals. The previous studies on gold electrodes were able to block the nonfaradaic background current using close-packed self-assembled monolayer of small passivating alkane thiol molecules. The covalent bond of small passivating molecules does not allow them to move around to form a close-packed monolayer. Thus there were many leaking pinholes in the passivation layer on GCE. This is even more severe on VACNF NEA due to the curvature and inhomogeneity at the CNF surface. As a result, it was not possible to use CV to measure the Fc signal on VACNF NEAs. ACV provides a necessary solution for the reported enzymatic study.

While we have demonstrated that it is feasible to detect the enzymatic kinetics of both legumain and cathepsin B. It remains critical to evaluate the specificity for any practical applications. This will be carefully investigated in the future. Our preliminary data indicated that the specificity of protease detection using this reported method strongly depended on the value of the "specificity constant" k_{cat}/K_M. Cathepsin B has higher k_{cat}/K_M which resulted in ~75% of drop in the electrochemical signal due to cleavage to the designated tetrapeptide (see Figure 4). As a result, the exponential decay can be reliably measured, giving high specificity. In contrast, as shown in Figure S16, the change of electrochemical signal is negligible using a tetrapeptide without Arg. For legumain, the low value of k_{cat}/K_M caused that the electrochemical signal only dropped by ~10% (see Figure 6a). The disturbance to the electrode during adding the enzyme solution caused uncontrollable fluctuation in the electrochemical signal. This limited precisely deriving the k_{cat}/K_M value. Therefore, the specificity for legumain is inconclusive at this stage and needs careful further study. But we can conclude that k_{cat}/K_M of $(1.13 \pm 0.38) \times 10^4$ $M^{-1}s^{-1}$ (as for legumain) is about the low limit for reliable protease measurements using the current setup.

Conclusions

In summary, we have demonstrated that high-frequency ACV can be applied on embedded VACNF NEAs to measure the redox reaction of Fc attached to the exposed CNF tip through a tetrapeptide and linker molecule. Due to the additional capacitive current pathway enabled by the unique interior graphitic microstructure of the VACNFs, the optimum frequency giving the highest peak AC current for Fc on VACNF NEA was found to be 40 times of that on GCEs. The higher frequency afforded a larger ACV signal and shorter time for the each ACV measurements. Thus the kinetics of proteolysis of the surface-attached peptides can be measured upon addition of two types of cancer related proteases, i.e. legumain and cathepsin B. The kinetic process can be analyzed with a heterogeneous Michaelis-Menten model to derive the "specificity constant" k_{cat}/K_m, which is $(4.3 \pm 0.8) \times 10^4$ $M^{-1}s^{-1}$ for cathepsin B and $(1.13 \pm 0.38) \times 10^4$ $M^{-1}s^{-1}$ for legumain. These values are about 2 times of that measured with a fluorescence assay as well as the specifications provided by the vendor. The nanostructured electrode size clearly eliminated the steric effects for enzymatic reactions with surface-attached peptides. This is the first example of the use of VACNF NEA on protease activity study. These VACNF NEA based electrochemical enzymatic biosensors can be potentially developed into portable multiplex electronic devices for rapid cancer diagnosis and treatment monitoring. Further study on the specificity and sensitivity of this VACNF NEA biosensor applied with biological samples is in progress toward this goal.

Supplementary Material

Refer to Web version on PubMed Central for supplementary material.

Acknowledgments

This work was supported by Award Number R15CA159250 from the National Cancer Institute, and, in part, by grant number P20RR015563 from the National Center for Research Resources and by Johnson Center for Basic Cancer Research at Kansas State University. The content of this article is solely the responsibility of the authors and does not necessarily represent the official views of the NCI or the NIH.

References

1. Carmeliet P. Angiogenesis in Health and Disease. Nat Med. 2003; 9:653–660. [PubMed: 12778163]
2. Koblinski JE, Ahram M, Sloane BF. Unraveling the Role of Proteases in Cancer. Clin Chim Acta. 2000; 291:113–135. [PubMed: 10675719]
3. Puente XS, Sanchez LM, Overall CM, Lopez-Otin C. Human and Mouse Proteases: a Comparative Genomic Approach. Nat Rev Genet. 2003; 4:544–558. [PubMed: 12838346]
4. Murthy RV, Arbman G, Gao J, Roodman GD, Sun X. Legumain Expression in Relation to Clinicopathologic and Biological Variables in Colorectal Cancer. Clin Cancer Res. 2005; 11:2293–2299. [PubMed: 15788679]
5. Shirahama-Noda K, Yamamoto A, Sugihara K, Hashimoto N, Asano M, Nishimura M, Hara-Nishimura I. Biosynthetic Processing of Cathepsins and Lysosomal Degradation are Abolished in Asparaginyl Endopeptidase-Deficient Mice. J Biol Chem. 2003; 278:33194–33199. [PubMed: 12775715]
6. Mattock KL, Gough PJ, Humphries J, Burnand K, Patel L, Suckling KE, Cuello F, Watts C, Gautel M, Avkiran M, et al. Legumain and Cathepsin-L Expression in Human Unstable Carotid Plaque. Atherosclerosis. 2010; 208:83–89. [PubMed: 19671471]
7. Gawenda J, Traub F, Lück H, Kreipe H, von Wasielewski R. Legumain Expression as a Prognostic Factor in Breast Cancer Patients. Breast Cancer Res Treat. 2007; 102:1–6. [PubMed: 17028987]
8. Briggs J, Haugen M, Johansen H, Riker A, Abrahamson M, Fodstad O, Maelandsmo G, Solberg R. Cystatin E/M Suppresses Legumain Activity and Invasion of Human Melanoma. BMC Cancer. 2010; 10:17. [PubMed: 20074384]
9. Turk B. Targeting Proteases: Successes, Failures and Future Prospects. Nat Rev Drug Discov. 2006; 5:785–799. [PubMed: 16955069]
10. Tang Z, Wu H, Zhang Y, Li Z, Lin Y. Enzyme-Mimic Activity of Ferric Nano-Core Residing in Ferritin and Its Biosensing Applications. Analytical Chemistry. 2011; 83:8611–8616. [PubMed: 21910434]
11. Shimura K, Kasai K, Matsumoto H. Assay of Trypsin Activity by Capillary Isoelectric Focusing with Laser-Induced Fluorescence Detection. Electrophoresis. 1998; 19:2296–2300. [PubMed: 9788312]
12. Vestling MM, Murphy CM, Fenselau C. Recognition of Trypsin Autolysis Products by High-Performance Liquid Chromatography and Mass Spectrometry. Anal Chem. 1990; 62:2391–2394. [PubMed: 2291484]
13. Orosco MM, Pacholski C, Miskelly GM, Sailor MJ. Protein-Coated Porous-Silicon Photonic Crystals for Amplified Optical Detection of Protease Activity. Adv Mater. 2006; 18:1393–1396.
14. Hook VY, Schiller MR, Nguye C, Yasothornsrikul S. Production of Radiolabeled Neuropeptide Precursors by in Vitro Transcription and Translation. Pept Res. 1996; 9:183–187. [PubMed: 8914165]
15. Adjemian J, Anne A, Cauet G, Demaille C. Cleavage-Sensing Redox Peptide Monolayers for the Rapid Measurement of the Proteolytic Activity of Trypsin and α-Thrombin Enzymes. Langmuir. 2010; 26:10347–10356. [PubMed: 20329721]
16. Ohtsuka K, Maekawa I, Waki M, Takenaka S. Electrochemical Assay of Plasmin Activity and Its Kinetic Analysis. Anal Biochem. 2009; 385:293–299. [PubMed: 19041631]

17. Penner RM, Heben MJ, Longin TL, Lewis NS. Fabrication and Use of Nanometer-Sized Electrodes in Electrochemistry. Science. 1990; 250:1118–1121. [PubMed: 17840192]
18. Fan FR, Bard AJ. Electrochemical Detection of Single Molecules. Science. 1995; 267:871–874. [PubMed: 17813918]
19. Menon VP, Martin CR. Fabrication and Evaluation of Nanoelectrode Ensembles. Anal Chem. 1995; 67:1920–1928.
20. Wei D, Bailey MJA, Andrew P, Ryhanen T. Electrochemical Biosensors at The Nanoscale. Lab Chip. 2009; 9:2123–2131. [PubMed: 19606287]
21. Lapierre-Devlin MA, Asher CL, Taft BJ, Gasparac R, Roberts MA, Kelley SO. Amplified Electrocatalysis at DNA-Modified Nanowires. Nano Lett. 2005; 5:1051–1055. [PubMed: 15943441]
22. Lanyon YH, De Marzi G, Watson YE, Quinn AJ, Gleeson JP, Redmond G, Arrigan DWM. Fabrication of Nanopore Array Electrodes by Focused Ion Beam Milling. Anal Chem. 2007; 79:3048–3055. [PubMed: 17370998]
23. Li H, Wu N. A Large-Area Nanoscale Gold Hemisphere Pattern as a Nanoelectrode Array. Nanotechnology. 2008; 19:275301. [PubMed: 21828697]
24. Li J, Koehne JE, Cassell AM, Chen H, Ng HT, Ye Q, Fan W, Han J, Meyyappan M. Inlaid Multi-Walled Carbon Nanotube Nanoelectrode Arrays for Electroanalysis. Electroanalysis. 2005; 17:15–27.
25. Lin Y, Lu F, Tu Y, Ren Z. Glucose Biosensors Based On Carbon Nanotube Nanoelectrode Ensembles. Nano Lett. 2004; 4:191–195.
26. Baker SE, Tse KY, Lee CS, Hamers RJ. Fabrication and Characterization of Vertically Aligned Carbon Nanofiber Electrodes for Biosensing Applications. Diamond Relat Mater. 2006; 15:433–439.
27. Arumugam PU, Chen H, Siddiqui S, Weinrich JAP, Jejelowo A, Li J, Meyyappan M. Wafer-scale Fabrication of Patterned Carbon Nanofiber Nanoelectrode Arrays: a Route for Development of Multiplexed, Ultrasensitive Disposable Biosensors. Biosens Bioelectron. 2009; 24:2818–2824. [PubMed: 19303281]
28. Li J, Ng HT, Cassell A, Fan W, Chen H, Ye Q, Koehne J, Han J, Meyyappan M. Carbon Nanotube Nanoelectrode Array for Ultrasensitive DNA Detection. Nano Lett. 2003; 3:597–602.
29. Koehne JE, Marsh M, Boakye A, Douglas B, Kim IY, Chang SY, Jang DP, Bennet KE, Kimble C, Andrews R, et al. Carbon Nanofiber Electrode Array for Electrochemical Detection of Dopamine Using Fast Scan Cyclic Voltammetry. Analyst. 2010; 136:1802–1805. [PubMed: 21387028]
30. Yu Z, McKnight TE, Ericson MN, Melechko AV, Simpson ML, Morrison B. Vertically Aligned Carbon Nanofiber Arrays Record Electrophysiological Signals From Hippocampal Slices. Nano Lett. 2007; 7:2188–2195. [PubMed: 17604402]
31. McKnight TE, Melechko AV, Hensley DK, Mann DGJ, Griffin GD, Simpson ML. Tracking Gene Expression After DNA Delivery Using Spatially Indexed Nanofiber Arrays. Nano Lett. 2004; 4:1213–1219.
32. Koehne J, Li J, Cassell AM, Chen H, Ye Q, Ng HT, Han J, Meyyappan M. The Fabrication and Electrochemical Characterization of Carbon Nanotube Nanoelectrode Arrays. J Mater Chem. 2004; 14:676–684.
33. Banks CE, Davies TJ, Wildgoose GG, Compton RG. Electrocatalysis at Graphite and Carbon Nanotube Modified Electrodes: Edge-Plane sites and Tube Ends are the Reactive Sites. Chem Commun. 2005; 2005:829–841.
34. Syed LU, Liu J, Prior AM, Hua DH, Li J. Enhanced Electron Transfer Rates by AC Voltammetry for Ferrocenes Attached to the End of Embedded Carbon Nanofiber Nanoelectrode Arrays. Electroanalysis. 2011; 23:1709–1717.
35. Beer PD, Smith DK. Tunable Bis(ferrocenyl) Receptors for the Solution-Phase Electrochemical Sensing of Transition-Metal Cations. J Chem Soc, Dalton Trans. 1988:417.
36. Li J, Ng HT, Cassell A, Fan W, Chen H, Ye Q, Koehne J, Han J, Meyyappan M. Carbon Nanotube Nanoelectrode Array for Ultrasensitive DNA Detection. Nano Letters. 2003; 3:597–602.
37. Gutiérrez OA, Chavez M, Lissi E. A Theoretical Approach to Some Analytical Properties of Heterogeneous Enzymatic Assays. Anal Chem. 2004; 76:2664–2668. [PubMed: 15117213]

38. Creager S, Yu CJ, Bamdad C, O'Connor S, MacLean T, Lam E, Chong Y, Olsen GT, Luo J, Gozin M, et al. Electron Transfer at Electrodes Through Conjugated "Molecular Wire" Bridges. J Am Chem Soc. 1999; 121:1059–1064.

39. Almeida PC, Oliveira V, Chagas JR, Meldal M, Juliano MA, Juliano L. Hydrolysis by Cathepsin B of Fluorescent Peptides Derived From Human Prorenin. Hypertension. 2000; 35:1278–1283. [PubMed: 10856277]

40. Nägler DK, Storer AC, Portaro FCV, Carmona E, Juliano L, Ménard R. Major Increase in Endopeptidase Activity of Human Cathepsin B upon Removal of Occluding Loop Contacts. Biochemistry. 1997; 36:12608–12615. [PubMed: 9376367]

41. Therrien C, Lachance P, Sulea T, Purisima EO, Qi H, Ziomek E, Alvarez-Hernandez A, Roush WR, Menard R. Cathepsins X and B Can Be Differentiated Through Their Respective Mono- and Dipeptidyl Carboxypeptidase Activities. Biochemistry. 2001; 40:2702–2711. [PubMed: 11258881]

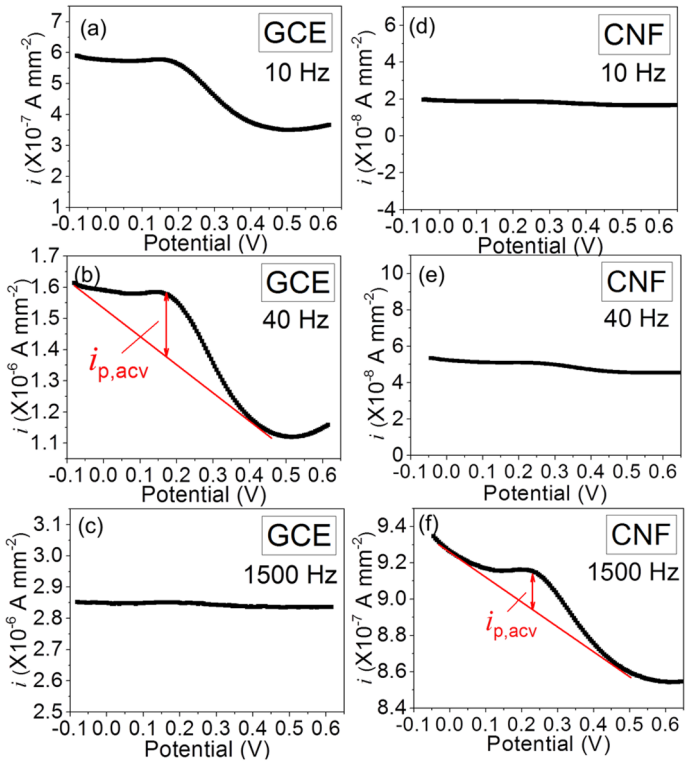

Figure 1.

Comparison of AC voltammograms (ACVs) measured at 10, 40 and 1500 Hz of H_2N-$(CH_2)_4$-CO-Ala-Ala-Asn-Leu-$NHCH_2$-Fc immobilized on a macro-GCE (a–c) and on a VACNF NEA (d–f). All the measurements were done in 500 μL of 50 mM MES (pH 5.0) and 250 mM NaCl. Sinusoidal waves with the fixed amplitude of 25 mV were superimposed on a DC staircase ramp from −0.05 to +0.65 V at a scan rate of 10 $mV•s^{-1}$. The measured average AC current at each point was normalized by the 7.1 mm^2 geometric surface area defined by the 3-mm i.d. Oring. The actual CNF surface area is ~100 times less.

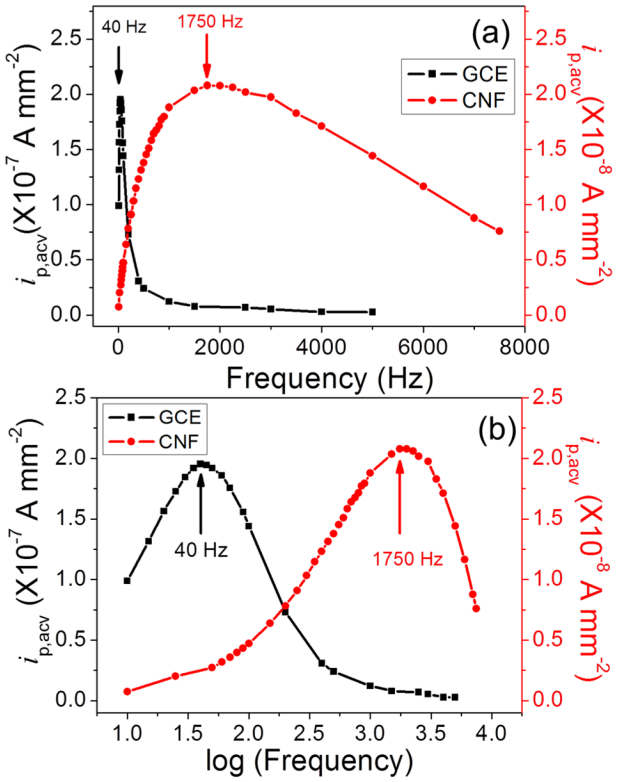

Figure 2.

(a) Background-corrected ACV peak current density $i_{p,acv}$ (normalized to the 7.1 mm^2 geometric electrode area) of H_2N-$(CH_2)_4$-CO-Ala-Ala-Asn-Leu-$NHCH_2$-Fc immobilized on a GCE (square) and a VACNF NEA (filled circle) plotted against the AC frequency. (b) Plot of $i_{p,acv}$ versus logarithm of the AC frequency. Note: The real CNF surface area is ~100 times less than the geometric surface area defined by the O-ring.

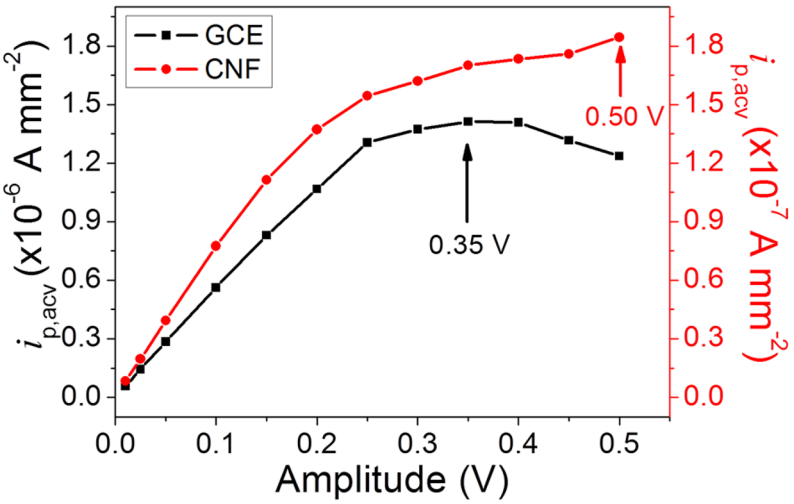

Figure 3.

Background-corrected ACV peak current density $i_{p,acv}$ (normalized to the 7.1 mm^2 geometric electrode area) of H_2N-$(CH_2)_4$-CO-Ala-Ala-Asn-Leu-$NHCH_2$-Fc immobilized on a GCE and a VACNF NEA plotted against the amplitude of the AC voltage (square: GCE, filled circle: VACNF NEA).

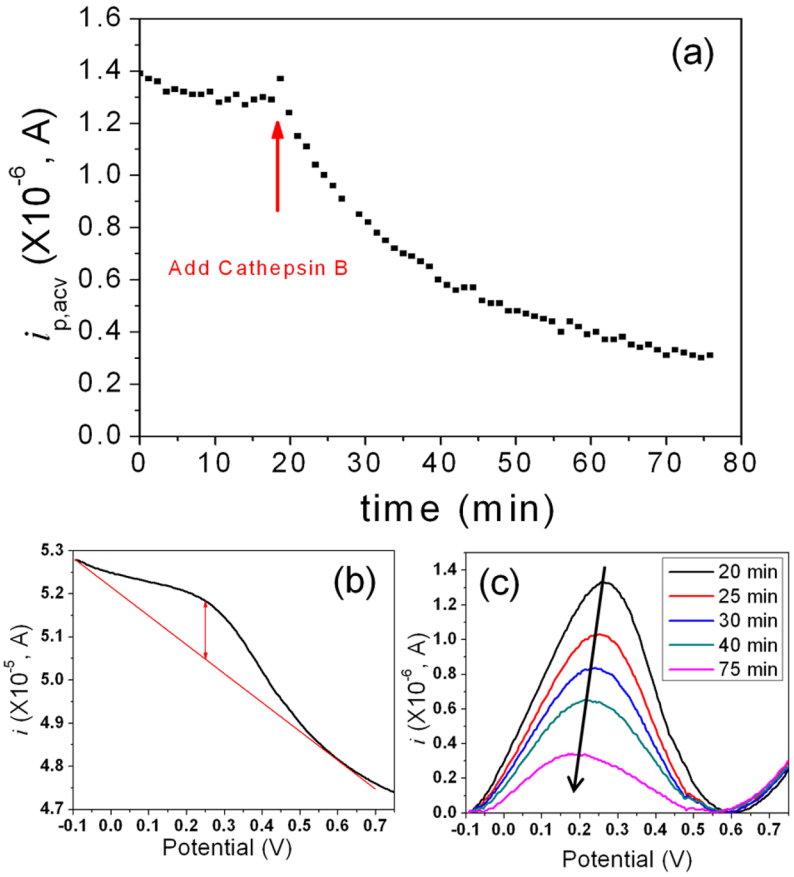

Figure 4.

(a) The change of the peak current ($i_{p,acv}$) of H_2N-$(CH_2)_4$-CO-Leu-Arg-Phe-Gly-NH-CH_2-Fc immobilized on a VACNF NEA in continuously repeated ACV measurements while 25 μL of 9.8 ng•μL^{-1} (338 nM) cathepsin B in the activation buffer consisting of 5 mM DTT and 25 mM MES (pH 5.0) was added into the electrochemical cell containing 250 μL of 25 mM MES (pH 5.0). All ACV measurements were carried out at f = 800 Hz and AC voltage amplitude V_0 = 150 mV. (b) ACV curve measured at the time of 20 minute immediately after the cathepsin B solution was added into the electrochemical cell. (c) Five representative background-subtracted ACV curves measured at 20 (black), 25 (red), 30 (blue), 40 (green) and 75 minute (pink), respectively, showing the decrease of $i_{p,\,acv}$ due to enzymatic cleavage

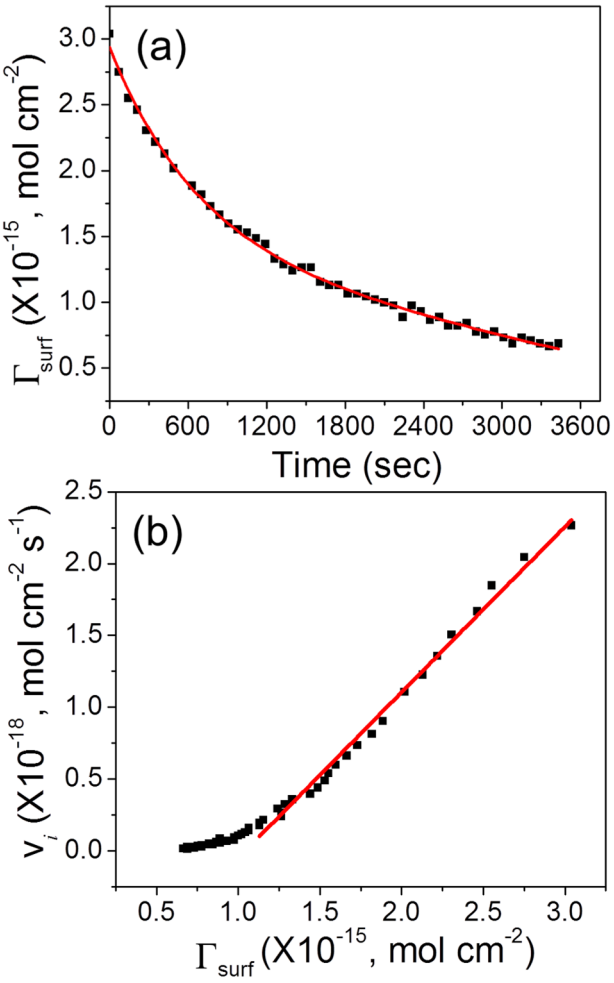

Figure 5.

Replot of the data presented in Figure 4. (a) Decrease of the quantity of surface adsorbed Fc (i.e. Γ_{surf}) during enzymatic cleavage of the tetrapeptide after adding the cathepsin B solution. (b) Plot of the reaction rate (v_i) versus the quantity of surface adsorbed Fc (Γ_{surf}) during the enzymatic reaction.

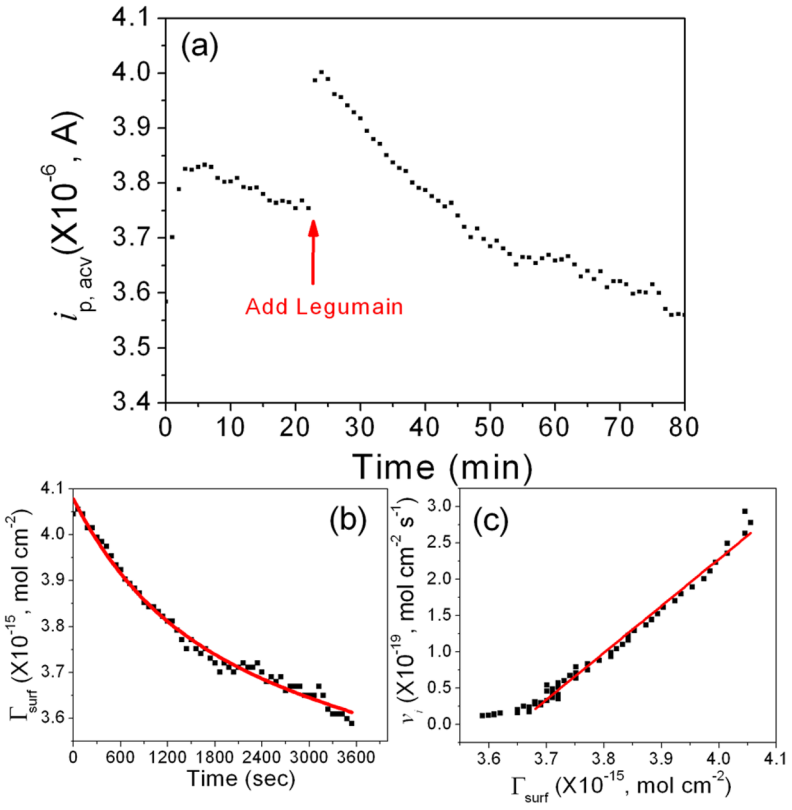

Figure 6.

(a) The change of the peak current ($i_{p,acv}$) of H_2N-$(CH_2)_4$-CO-Ala-Ala-Asn-Leu-NH-CH_2-Fc immobilized on a VACNF NEA in continuously repeated ACV measurements while 11 μL of 90.9 ng μL^{-1} (1.90 μM) legumain in the activation buffer consisting of 50 mM CH_3COONa (pH = 4.0, adjusted by adding acetic acid) and 100 mM NaCl was added into the electrochemical cell containing 250 μL of 50 mM MES (pH 5.0) and 250 mM NaCl. All ACV measurements were carried out at f = 1750 Hz and AC voltage amplitude V_0 = 150 mV. (b) Replot of the data presented in figure (a) showing the reduction of the quantity of surface adsorbed Fc (i.e. Γ_{surf}) during enzymatic cleavage of the tetrapeptide after adding the legumain. (c) Plot of the reaction rate (v_i) versus the quantity of surface adsorbed Fc (Γ_{surf}) during the enzymatic reaction.

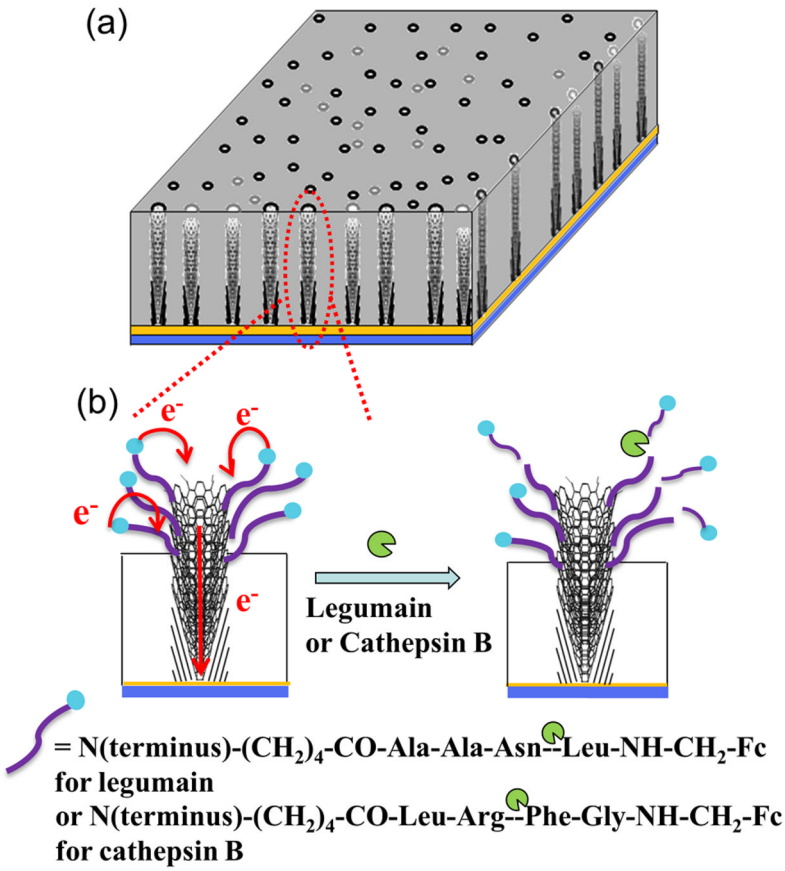

Scheme 1.

Schematic diagram of the cleavage of Fc-linked tetrapeptides at the VACNF NEA tip by specific proteases. (a) A random VACNF array embedded in the SiO_2 matrix. (b) Electron transfer from appended ferrocene at the distal end of the peptide to the underlying metal film electrode through the VACNFs and the loss of the electrochemical signal from ferrocene due to the cleavage of the peptide at specific sites.

Table 1

Comparison of the specificity constant k_{cat}/K_m for legumain and cathepsin B, derived from the electrochemical method (i.e. ACV on VACNF NEAs) and the fluorescence assay in solutions.

Enzyme	Peptide Sequence	k_{cat}/K_m ($M^{-1}s^{-1}$)
Legumain	(FL[a]) Ala-Ala-Asn↓AMC	$(4.3 \pm 0.6) \times 10^3$
	(EC[b]) Ala-Ala-Asn↓Leu-NH-CH_2-Fc	$(11.3 \pm 3.8) \times 10^3$
Cathepsin B	(FL) Leu-Arg↓AMC	$(2.3 \pm 1.7) \times 10^4$
	(EC) Leu-Arg↓Phe-Gly-NH-CH_2-Fc	$(4.3 \pm 0.8) \times 10^4$

[a]FL: fluorescence; ↓: cleavage site. The fluorescence data were derived from the analysis in Figures S8, S9, S11 and S12.

[b]EC: electrochemistry. The electrochemical data were statistical value over at least duplicated experiments.